http://dx.doi.org/10.5012/bkcs.2012.33.12.4155

Effects of the Superlattices on STM Imaging of Self-organized Substituted Alkyl Chain Monolayers on a Graphite Surface

Seung Bae Son and Jae Ryang Hahn*

*Department of Chemistry and Research Institute of Physics and Chemistry, Chonbuk National University, Jeonju 561-756, Korea. *E-mail: jrhahn@jbnu.ac.kr*
Received June 27, 2012, Accepted September 28, 2012

We characterized the physisorption of *p*-iodo-phenyl octadecyl ether molecules (I-POE) onto superlattice regions of graphite surfaces using scanning tunneling microscopy (STM). The formation of self-organized I-POE monolayers does not affect the overall structures of moiré patterns and their modulation periods. However, the packing density of the I-POE monolayer and the orientations of lamella structures were sensitive to the underlying superlattice structure. Depending on the bias voltage, the STM images selectively showed moiré pattern, I-POE layer, or both. Reflecting the local density of states at a certain energy level, the STM images thereby revealed the relative energy level scale of the superlattice with respect to the molecular orbitals of I-POE.

Key Words : Scanning tunneling microscopy, Graphite, Superlattice, Solid-liquid interface

Introduction

Highly oriented pyrolytic graphite (HOPG) is one of the most common substrates used in scanning tunneling microscopy (STM) experiments because it is chemically inert, commercially available, it displays atomically flat terraces, and it is easy to cleave, yielding fresh surfaces. The flat terraces and chemical inertness of the graphite surface have made it a popular substrate for preparing physisorbed organic molecular monolayers.[1-11] The chemical inertness of the graphite surface is advantageous for such studies because the essential physicochemical characteristics of the organic monolayer are presumably preserved, even upon adsorption. The structures of model organic monolayers on graphite surfaces ideally provide information relevant to thin film-based molecular electronics, lubricants, nano-patterned surfaces, and detergents.

In practice, graphite surfaces present a variety of defects,[12-18] and one must be careful in distinguishing defects from the features of adsorbed molecules. Therefore, it is important to develop a detailed understanding of the graphite defect surface features and how they affect the structures of adsorbates. Several distinct features of graphite surfaces may be readily observed in STM images. Large-scale surface corrugations are frequently present on the surfaces, possibly due to tip contamination effects.[12] The large observed corrugations were thought to arise from elastic deformations caused by the atomic force between the STM tip and the graphite surface.[13] A $\sqrt{3} \times \sqrt{3}$ R30° superlattice was detected around point defects or absorbed molecules that caused long-range electronic perturbations and gave rise to structural reconstructions.[16,19] Giant hexagonal periodic patterns with periodicities from a few to tens of nm, referred to as Moiré patterns, can extend over hundreds of nanometers.[20-31] These superperiodic patterns were previously attributed to misorientations in the surface layer with respect to the second layer of graphite, or to subsurface arrays of nanoscale defects.[20-23] Superperiodic superlattices may be randomly distributed on graphite surfaces and can potentially misguide the structures of the molecular adsorbates, particularly in the context of organic monolayers. Although graphite surfaces display unusual structures that differ from the well-known hexagonal patterns, few studies have examined how such structures affect the structures of molecular adsorbates.

In this work we investigated the physisorption of *p*-iodo-phenyl octadecyl ether molecules (I-POE) on graphite superlattice surfaces. We directly imaged monolayers of I-POE adsorbed to either pristine or superlattice regions of a graphite surface using STM. The periodic electron density of the superlattice was overlapped to the electron density of the I-POE monolayer in the STM images. The packing density of the monolayer and the orientations of I-POE lamella structures could be modified depending on the superlattice. The voltage-dependent STM images revealed the relative scales of the molecular orbital (MO) energy levels for I-POE and the density of states of the superlattice. Our observations suggest that the graphite superlattice can affect the STM images of organic monolayers and packing patterns, contradicting the assumption of chemical inertness on the pristine graphite surfaces.

Experimental

The I-POE molecules were synthesized according to a modified Williamson ether synthesis.[32] The structures and purities of each compound were confirmed by ^{1}H NMR and GC/MS. Pure, concentrated, unsaturated 1-phenylhexane solutions of I-POE were prepared (3.0 wt %). Physisorbed self-organized monolayers of I-POE were obtained by depositing a droplet of the solution on the basal plane of

graphite. STM measurements were carried out using a commercial STM (SOLVER P-47, NT-MDT) *in situ* at the liquid-solid interface. The HOPG (NT-MDT, grade ZYA) substrates were cleaved in air, and the STM images were collected under ambient conditions. The graphite surface was imaged by STM to confirm the high resolution of the tip. The superlattice areas were selected at random. The densities of the superlattice areas depended on the quality of the graphite and/or the number of solution treatments. When a large superlattice area was identified, the STM tip was retracted by the scanner piezo control, and a drop of I-POE solution was applied to the surface. The same scan area was then observed once the tip was restored to the tunneling position, as by the presence of markers, such as a line step or other large unusual structures. The tips were mechanically cut from a 0.20 mm Pt/Ir (80:20) wire. A constant current mode (topographical imaging) was employed for investigating the static properties of the structures. All images shown are the raw data with the mean plane subtracted.

Results and Discussion

Observation of the Moiré Patterns. Moiré patterns have been observed after deposition of metal atoms,[20] treatment with organic solvents,[30] or repeated trials using an adhesive tape.[31] The treatment of graphite samples in solution (or solvent) facilitates the formation of Moiré patterns. STM imaging can easily capture the patterns, which extend over a limited surface area. In this work, the 1-phenylhexane solvent also facilitated Moiré pattern formation, as clearly observed in the STM images (Fig. 1). Imaging the same region on the surface before and after the solvent treatment, we found that ~50% of pristine surface area was converted to Moiré patterns. The experimental observations showed a variety of Moiré patterns on the surfaces with superperiodicities ranging from 3 nm to 25 nm. Figures 1(a-c) show Moiré patterns with periodicities of 9.22 nm, 7.83 nm, and 3.83 nm, respectively. A closer look at the Moiré pattern area shown in Figure 1(a) reveals the presence of a smaller lattice structure overlapping the superlattice. The smaller lattice structure resembled the trigonal asymmetric patterns observed in STM images of pristine graphite surfaces. The lattice spacing was 0.25 nm, which agreed well with the triangular lattice constant of pristine graphite. This observation contrasted with other reports of curved and wavy lattice rows of smaller lattice structures in the superlattice area.[20,26]

Moiré patterns are produced by the rotation of a surface layer with respect to the underlying layer in a graphite crystal. The rotational effects that give rise to the Moiré patterns decay rapidly from the surface layer into the bulk. The attenuation factor is around 2.6.[21,31] For simplicity, we assumed that the top two layers generated the Moiré pattern. Suppose that θ is the relative rotational angle and D is the periodicity of the Moiré pattern. Then we have: $D = d/[2\sin(\theta/2)]$, where d is the triangular structure lattice constant (0.246 nm) of the graphite surface.[21,25] According to this formula and the experimentally measured periodicities of the Moiré pattern given in Figures 1(a-c), the rotational angles were calculated to be about 1.54°, 1.80°, and 3.68°, respectively. The rotation angles were used to simulate models of the graphite superlattice. Figures 1(d-f) show models of the superlattices with the same periodicities as were observed in the experimental images shown in Figures 1(a-c). Three sites are indicated in Figure 1(e): M-β, M-α, and M-h sites. The M-β sites of the Moiré pattern were the brightest features because the atoms of the M-β sites were located above hole sites.[20] Likewise, the M-α sites were expected to be the second brightest features, whereas the M-h sites were the darkest features, as shown in Figures 1(a-c).

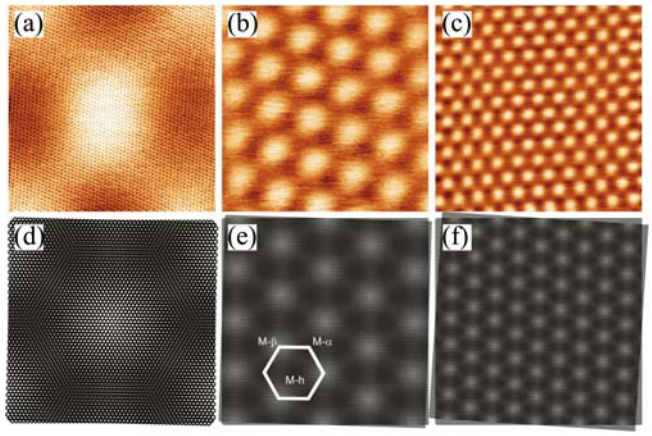

Figure 1. (a)-(c) STM topographical images of various superlattices obtained on HOPG surfaces. The scan area was 12 × 12 nm^2 for image (a) and 30 × 30 nm^2 for images (b) and (c). The sample bias voltages and tunneling currents were: (a) 50 mV and 100 pA; (b) 50 mV and 80 pA; and (c) 10 mV and 100 pA. The periodicities of the superlattice (D) were 9.22 nm, 7.83 nm, and 3.83 nm for images (a)-(c), respectively. Thermal drift was not compensated for in the STM images. (d)-(f) Simulated Moiré patterns formed by two hexagonal graphite layers that overlapped with a misorientation. The patterns were simulated under the (experimentally obtained) periodicity conditions and rotation angles of (θ): (d) D = 9.22 nm, θ = 1.54°; (e) D = 7.83 nm, θ = 1.80°; and (f) D = 3.83 nm, θ = 3.68°, and corresponded to the STM images (a)-(c), respectively. Three distinct graphite superlattice sites are indicated in Figure 1(e) (M-β-site, M-α-site, and M-h-site).

Self-organized I-POE Monolayers on Superlattices. A droplet of liquid I-POE was deposited onto pristine or superlattice regions to investigate the effects of the superlattice on the organic monolayer. Self-organized monolayers of I-POE formed with stable single 2-D-crystalline domains as large as a few thousand nm^2 on the pristine graphite surface. Figure 2(a) shows a topographical image of the I-POE monolayers formed on a pristine graphite surface from a 3.0 wt % solution in 1-phenylhexane. Once formed, the I-POE monolayers remained stable for STM imaging. The I-POE molecules in the images consisted of one large bright spot per I-POE molecule with an approximate periodicity of 29.3 (± 1) Å. The bright spots corresponded to the head groups of the molecules (iodine atom, phenyl ring, and oxygen atom), and the less bright rows corresponded to the alkyl chains. The distance between adjacent alkyl chains of the I-POE molecules was determined to be 9 (± 1) Å, larger than the di-

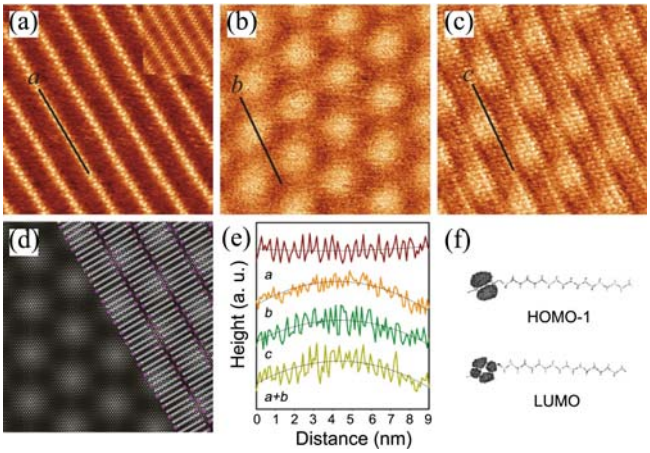

Figure 2. (a) STM topographical images of an I-POE (scan area: 20 × 20 nm^2) monolayer formed at the liquid-graphite interface at a pristine graphite surface (not a superlattice), revealing the head-to-tail configurations of the molecules. This image was obtained at a tunneling current of 30 pA and a sample bias voltage of –600 nV. The carbon chains were revealed under different tunneling conditions (inset image): a tunneling current of 45 pA and a bias voltage of –550 nV. (b) STM image of a graphite superlattice (20 × 20 nm^2) obtained at a tunneling current of 60 pA and a bias voltage of 100 nV, showing a periodicity of D = 5 nm. (c) On the same superlattice surface of image (b), a droplet of I-POE solution was deposited and rescanned at a tunneling current of 25 pA and a bias voltage of 100 nV. (d) A simulation model corresponding to Figure 2(c) with parameters D = 5 nm, θ = 2.80°. (e) Cross-sectional cuts drawn along the lines indicated in Figures 2(a)-(c). (f) MO electron density contours (HyperChem AM1 method) of the HOMO and LUMO structures of I-POE.

stances between *n*-alkanes (4.2 Å).[33] Such a large separation arose from the bulky I-POE head groups. The alkyl chain axes were oriented parallel to the graphite plane under different tunneling conditions (inset). The length of the head groups was 7 (± 0.5) Å and the length of the alkyl chain was 22.2 (± 1) Å. These geometric factors were consistent with the values calculated using HyperChem, within a 1 Å resolution. The molecules were generally organized in a head-to-tail configuration. Occasionally, adjacent molecules were shifted from one another (not shown), presumably to reduce the steric hindrance among neighboring head groups. This configuration might lead to a lower surface energy, possibly owing to the cancellation of the net molecular dipole. The length scales of the head groups are different from the underlying graphite lattice. This mismatch was readily observed on each contour of the STM image.

Figure 2(f) shows two calculated MOs of the I-POE molecule. The electron densities of the highest occupied molecular orbital (HOMO-1) and the lowest unoccupied molecular orbital (LUMO) levels were highest at the phenyl group. A comparison of STM images of the adsorbed I-POE molecules with the electron density contours calculated using HyperChem suggested tunneling of the individual bonding MOs. The bright features in the STM image corresponded to the HOMO of the phenyl ring substituents in the I-POE molecules. Previously it was observed that the number of bright spots per head group in STM image depended on the bias voltage, corresponding to the bias-dependent participation in tunneling of the individual bonding MOs.[10,11]

Figure 2(b) shows a region of the graphite superlattice that resembled the trigonal asymmetric protrusions of a pristine graphite surface, except that the lattice periodicity differed. The superlattice had a periodicity of 5.00 nm and a corresponding rotational misorientation of 2.8°. A droplet of liquid I-POE was deposited on this region and the surface was scanned once again (Fig. 2(c)). The I-POE monolayer modified the appearance of the superlattice in STM image, but the periodicity of the superlattice protrusions remained unchanged. The head-to-tail configuration did not change significantly; however, the head groups of the I-POE became brighter when they were aligned over the M-β-sites. A possible model of the monolayer structure is shown in Figure 2(d). Figure 2(e) shows the cross-sectional cuts along the lines on monolayers formed on either pristine (curve *a*, Fig. 2(a)) or superlattice (curve *c*, Fig. 2(c))) graphite surfaces, or along the line of a superlattice without a monolayer (curve *b*, Fig. 2(b)). The curve *a*+*b* in Figure 2(e) is the sum of the curves *a* and *b*. The overall shape of the sum was similar to the curve *c*, although the peak positions could not be directly compared in this work. This suggested that the electronic states of the I-POE monolayers were overlapped to the electronic structures of the graphite superlattice, yielding the image shown in Figure 2(c).

Effects of the Superlattices on the Packing Patterns of the I-POE Monolayers: The superlattice affected the packing patterns of the I-POE molecules on the graphite surfaces. Figure 3(a) shows a large-scale STM image of I-POE monolayers on either pristine or superlattice graphite surfaces. The area indicated by the black lines shows the boundary of the monolayer domain formed on the pristine graphite. Blue and red lines indicate the boundaries of I-POE monolayer domains formed on the superlattice. The superlattice had a periodicity of 8.71 nm. I-POE molecules of monolayers formed on two domains within the superlattice region were rotated relative to one another by 120°. Figures 3(b and c) show magnified images of the two domains. The black solid lines in the images were drawn along the head groups of the I-POE molecules. The head groups of I-POEs were well-aligned in one direction on the domain marked by the red lines (Fig. 3(c)), but the alignment of head groups on the domain indicated by the blue lines were frequently misaligned (Fig. 3(b)). These features indicated that the packing patterns of the I-POE on the superlattice may depend on the orientations of the lamella structures. Better alignment between the lamella structures and the superlattice may have required a lower packing energy. The misalignment of head groups was not observed on the pristine graphite surface, suggesting that coupling between the superlattice electronic structure and the molecular electronic structure could influence the packing pattern.

Interestingly, Moiré rotations can lead to the formation of a hexagonal honeycomb superlattice pattern, as shown in Figure 3(d). Moiré patterns generally arise from the rotation of the first layer relative to the second layer; however,

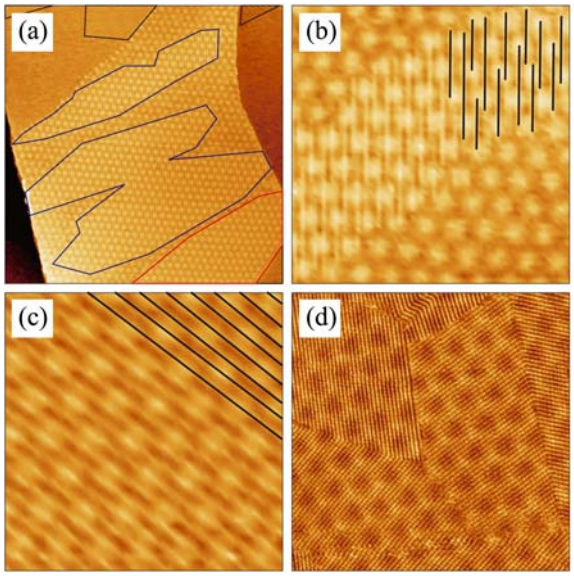

Figure 3. Effects of the superlattice on the packing patterns of the I-POE monolayer. (a) Large I-POE monolayer areas on a graphite superlattice (300 × 300 nm^2, D = 8.71 nm) and on pristine region, obtained at a tunneling current of 25 pA and a sample bias voltage of 100 nV. I-POE monolayers formed on a pristine graphite surface are indicated by black solid lines. The areas marked by blue and red lines indicate the I-POE monolayers formed on graphite superlattices. (b) and (c) show magnified views of the different packing patterns on a superlattice region. The black solid lines in images (b) and (c) were drawn along the head groups of the I-POE molecules. (d) I-POE monolayer formed on a superlattice region with a hexagonal pattern (200 × 200 nm^2, D = 22.02 nm). The scan conditions included a tunneling current of 20 pA and a bias voltage of 100 nV.

rotations of the second or third layers can also affect the superlattice pattern. Simulations revealed that the three-fold asymmetry of the superlattice generated by exaggerated weighting functions was not as pronounced as the asymmetries of the superlattice generated using normal weighting functions.[28] The superlattice indeed resembled a hexagonal pattern, although the cause of the rotations was not clear. Figure 3(d) shows an STM image of an I-POE monolayer formed on the hexagonal pattern of a graphite superlattice. The coverage of the I-POE monolayer increased significantly over the hexagonal superlattice area. As shown in Figure 3(a), several uncovered areas were observed between the domains on the trigonal asymmetric superlattice and the pristine graphite area; however, the I-POE monolayers were densely packed over the hexagonally patterned region (Fig. 3(d)). The average packing ratios (the fractional area of molecular domains) were 0.73(± 0.05) and 0.38(± 0.05) on the trigonal superlattice and pristine graphite regions, respectively, and 0.95(± 0.03) on the hexagonal superlattice region. No measurable differences were observed in the distance of I-POE molecules on the three regions.

Effects of the Sample Bias Voltages on the STM Images of the I-POE Monolayer. The STM images of the I-POE monolayer on a superlattice varied with the sample bias voltage. Figures 4(a-c) show STM images of a single region

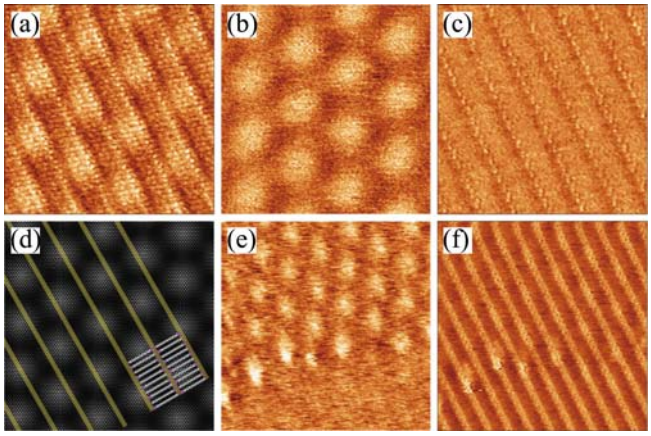

Figure 4. Effects of the tunneling parameters on the images of I-POE monolayers formed on a graphite superlattice. (a)-(c) STM images of an I-POE monolayer on the same region under different tunneling current and bias voltage scanning conditions (18 × 18 nm^2, D = 5.00 nm): (a) 30 pA, 100 nV; (b) 30 pA, –200 nV; and (c) 30 pA, –460 nV. (d) Simulated I-POE monolayers on graphite superlattices, corresponding to images (a)-(c). (e) and (f) Voltage-dependent STM images of an I-POE monolayer containing a superlattice boundary (30 × 30 nm^2, D = 5.30 nm). The images were obtained at a tunneling current of 80 pA and bias voltages of (e) –270 nV and (f) –600 nV.

containing an I-POE monolayer obtained at different sample voltages. The I-POE layer was deposited onto the superlattice with a superlattice periodicity of 5.00 nm. When the bias voltage was flipped while holding the tunneling current constant, distinct changes were observed in STM images. The I-POE layer and the superlattice were observed at 100 nV (Fig. 4(a)), but the I-POE layer became transparent at –200 nV (Fig. 4(b)). A reduction of the sample bias voltage from –200 nV to –460 nV resulted in the observation of I-POE molecule head groups only (Fig. 4(c)). Neither the graphite superlattice nor the carbon chains of the I-POE were observed under these bias conditions. Figures 4(e and f) show other examples in which the sample bias voltage could be tuned to alter the images. The images were obtained at 80 pA with sample bias voltages of –270 (Fig. 4(e)) or –600 nV (Fig. 4(f)). At a sample bias voltage of –270 nV, only the boundary of the superlattice pattern was observed. The head groups (or tail groups) appeared at –600 nV, although the superlattice was not observed.

The voltage dependence of the STM images differed for positive and negative sample bias voltages. At positive sample bias voltages, the STM images always revealed the overlapping of the I-POE electronic states with that of the superlattice. However, at negative sample bias voltages, the overlapping was observed only between –400 nV and –500 nV. I-POE molecules alone were observed at sample voltages less than –500 nV. Sample voltages less than –400 nV revealed the superlattice without the I-POE layer. The relative voltage scale differed slightly under different tunneling currents. Our observations were made under 20-80 pA tunneling currents.

STM images of the molecular adsorbates may have re-

flected three types of tunneling: tunneling from the conducting substrate, tunneling from the MOs of the adsorbates, and resonance tunneling. Tunneling from a conducting substrate was based on the local modulation of the substrate work function by the presence of polarizable adsorbates;[1] however, this model did not agree with the high-resolution images of the alkane monolayers on a graphite surface, which displayed bright spots corresponding to the methyl/methylene groups despite their small polarizability.[4,5] The STM images could also reflect the electron densities of the MOs of the adsorbates themselves.[6] STM images of alkylcyanobiphenyl molecules on graphite surfaces were observed, revealing that the biphenyl group and alkyl tail exhibited high and low contrast, respectively. The images were compared with the electron density contours calculated for the HOMO and LUMO of the compounds. The contours revealed contrast only for the biphenyl group and, therefore, did not support the additional contrast observed in the alkyl tails.

Resonant tunneling was suggested by the STM images of the uncoated DNA adsorbed onto HOPG.[7] The pressure between the tip apex and the sample was calculated to be 0.1-10 GPa, sufficiently large to shift the positions of the MOs of the adsorbates and induce resonance tunneling. This mechanism was invoked to explain the voltage-dependent STM images of liquid crystals on HOPG.[8] In their model, the physisorbed molecules were represented as a potential well between the tip and the substrate. The potential wells contained discrete adsorbate MO levels that were shifted in energy relative to those of the isolated molecules. The tunneling probability increased at the quantized energy levels in the well due to resonance tunneling effects.[9] Therefore, the energy levels of the adsorbate HOMO and LUMO were determined by controlling the sample (or tip) bias voltage. Bias-dependent STM images have been reported for molecular adsorbates on graphite, including liquid crystals[6,8] and functionalized alkanes.[2] The STM images displayed a feature contrast that was characteristic of the substrate at low bias voltages,[2,6,8] of the substrate and adsorbate at intermediate bias voltages,[2] and of the adsorbate alone at higher bias voltages.[2,6,8]

The MO calculations of I-POE on graphite[10] predicted that the energy of the LUMO was 0.139 eV and the five HOMO levels were calculated to fall between –9.097 and –11.034 eV. Because the STM images reflected the partial electron density distribution near the Fermi level of the sample, the energy levels provided the energies of the five bonding MOs (HOMO to HOMO-4) and of the LUMO of the I-POE. The STM images were compared with the energy-minimized electron density contours of the I-POE to understand the potential contribution of the molecular adsorbate MOs to image contrast. Both carbon chains and head (or tail) groups of the I-POE and superlattice appeared to participate in coupling, based on the images of specific HOMO and LUMO groups and filled or empty states of the superlattice; however, the head groups of an I-POE monolayer not present on a superlattice were revealed in the HOMO image, as shown in Figures 4(c and f), under larger negative sample voltages. Our observations revealed the relative scales of the energy levels of the superlattice periodic structures with respect to those of the HOMO and LUMO structures of I-POE. The energy levels of the empty graphite superlattice states were similar to the LUMO and displayed coupling in the STM images. On the other hand, the energy levels of the filled superlattice states were lower than those of the I-POE HOMO. In this work, however, the absolute energies of the HOMO and LUMO structures could not be extracted because the STM tunneling current was associated with overlap among the electronic structures in the junction of the tip-molecule0surface. It was very difficult to achieve constant tip conditions, and the scan conditions were varied to yield electronic structures. The sample bias voltage-dependent STM images observed in the present work also suggested that the tunneling process may occur through a resonance mechanism involving the energy states of the adsorbate, tip, and graphite superlattice. If the energy level of the tip, as controlled by the bias, was in the vicinity of the adsorbate energy levels, tunneling through those levels was achieved, and the STM images reflected the electron density of the adsorbate MOs.[10]

Conclusions

We directly observed organic monolayers adsorbed onto graphite superlattices using STM imaging techniques. The electron density of the superlattice was found to couple to the electron density of the I-POE monolayer in the STM images. The packing ratios and orientations of the I-POE lamella structures could be modified on the superlattice. The bias voltage-dependent STM images revealed the relative scale of the I-POE MO energy levels and the filled (and empty) states of the graphite superlattice. Our observations showed that the graphite superlattice can affect the STM images and the packing characteristics of an organic monolayer, unlike the relative inertness of flat pristine graphite surfaces. Care must be taken to avoid misinterpreting organic monolayer structures observed by STM on superlattice regions.

Acknowledgments. This work was supported by grants from the Korean government (NRF) (2010-0024254 and 2007-0056333) and by research funds of Chonbuk National University in 2012.

References

1. Spong, J. K.; Mizes, H. A.; LaComb, L. J., Jr.; Dovek, M. M.; Frommer, J. E.; Foster, J. S. *Nature* **1989**, *338*, 137.
2. Claypool, C. L.; Faglioni, F.; Goddard, W. A., III; Gray, H. B.; Lewis, N. S.; Marcus, R. A. *J. Phys. Chem. B* **1997**, *101*, 5978.
3. Xu, S. L.; Yin, S. X.; Liang, H. P.; Wang, C.; Wan, L. J.; Bai, C. L. *J. Phys. Chem. B* **2004**, *108*, 620.
4. McGonigal, G. C.; Bernhardt, R. H.; Thomson, D. J. *Appl. Phys. Lett.* **1990**, *57*, 28.
5. Watel, G.; Thibaudau, F.; Cousty, J. *Surf. Sci.* **1993**, *281*, L297.
6. Smith, D. P. E.; Hörber, J. K. H.; Binnig, G.; Nejoh, H. *Nature* **1990**, *344*, 641.
7. Lindsay, S. M.; Sankey, O. F.; Li, Y.; Herbst, C.; Rupprecht, A. *J. Phys. Chem.* **1990**, *94*, 4655.

8. Mizutani, W.; Shigeno, M.; Ono, M.; Kajimura, K. *Appl. Phys. Lett.* **1990**, *56*, 1974.
9. Azbel, M. Y. *Phys. Rev. B* **1983**, *28*, 4106.
10. Lee, H. S.; Iyengar, S.; Musselman, I. H. *Langmuir* **1998**, *14*, 7475.
11. Son, S. B.; Lee, H.; Jeon, I. C.; Park, S. K.; Hahn, J. R. *J. Nanosci. Nanotechnol.* **2006**, *6*, 2494.
12. Mamin, H. J.; Ganz, E.; Abraham, D. W.; Thomson, R. E.; Clarke, J. *Phys. Rev. B* **1986**. *34*, 9015.
13. Soler, J. M.; Baro, A. M.; Garcia, N.; Rohrer, H. *Phys. Rev. Lett.* **1986**, *57*, 444.
14. Clemmer, C. R.; Beebe, T. P., Jr. *Science* **1991**, *251*, 640.
15. Chang, H.; Bard, A. J. *Langmuir* **1991**, *7*, 1143.
16. Hahn, J. R.; Kang, H. *Phys. Rev. B* **1999**, *60*, 6007.
17. Hahn, J. R.; Kang, H.; Song, S.; Jeon, I. C. *Phys. Rev. B* **1996**, *53*, R1725.
18. Hahn, J. R.; Kang, H. *Surf. Sci.* **1996**, *357-358*, 165.
19. Banhart, F.; Kotakoski, J.; Krasheninnikov, A. V. *ACS Nano* **2011**, *5*, 26.
20. Xhie, J.; Sattler, K.; Ge, M.; Venkateswaran, N. *Phys. Rev. B* **1993**, *47*, 15835.
21. Sun, H. L.; Shen, Q. T.; Jia, J. F.; Zhang, Q. Z.; Xue, Q. K. *Surf. Sci.* **2003**, *542*, 94.
22. Rong, Z. Y.; Kuiper, P. *Phys. Rev. B* **1993**, *48*, 17427.
23. Kobayashi, K. *Phys. Rev. B* **1996**, *53*, 11091.
24. Kuwabara, M.; Clarke, D. R.; Smith, D. A. *Appl. Phys. Lett.* **1990**, *56*, 2396.
25. Cee, V. J.; Patrick, D. L.; Beebe, T. P., Jr. *Surf. Sci.* **1995**, *329*, 141.
26. Bernhardt, T. M.; Kaiser, B.; Rademann, K. *Surf. Sci.* **1998**, *408*, 86.
27. Osing, J.; Shvets, I. V. *Surf. Sci.* **1998**, *417*, 145.
28. Pong, W. T.; Durkan, C. *Jpn. J. Appl. Phys.* **2005**, *44*, 5365.
29. Pong, W. T.; Bendall, J.; Durkan, C. *Surf. Sci.* **2007**, *601*, 498.
30. Wang, Y.; Ye, Y.; Wu, K. *Surf. Sci.* **2006**, *600*, 729.
31. Rong, Z. Y. *Phys. Rev. B* **1994**, *50*, 1839.
32. Leonard, N. J.; Felley, D. L.; Nicolaides, E. D. *J. Am. Chem. Soc.* **1952**, *74*, 1700.
33. Couto, M. S.; Liu, X. Y.; Meekes, H.; Bennema, P. *J. Appl. Phys*. **1994**, *75*, 627.